THE JOURNAL OF PHYSICAL CHEMISTRY C

Article

pubs.acs.org/JPCC

Size Dependent Surface Charge Properties of Silica Nanoparticles

Murat Barisik,[†,§] Selcuk Atalay,[‡,§] Ali Beskok,[†] and Shizhi Qian[‡,*]

[†]Department of Mechanical Engineering, Lyle School of Engineering, Southern Methodist University, Dallas, Texas 75275, United States

[‡]Institute of Micro and Nanotechnology, Old Dominion University, Norfolk, Virginia 23529, United States

ABSTRACT: Nanoparticle surface charge density plays an important role in many applications, such as drug delivery and cellular uptake. In this study, surface charge properties of silica nanoparticles with different sizes are studied using a multi-ion surface charge-regulation model. In contrast to most previous studies utilizing constant surface charge, protonation and deprotonation surface reactions are used to obtain the local surface charge, which depends on the particle size and electrolyte solution properties, including the salt concentration and pH. For a fixed particle size, the magnitude of the surface charge typically increases with an increase in pH or background salt concentration. For fixed background salt concentration and pH, the magnitude of surface charge decreases with an increase in the particle size and reaches a constant when the particle size exceeds a critical value. Size dependent surface charge is further characterized by the ratio of electrical double layer thickness to the particle diameter, and the surface charge varies significantly when this dimensionless ratio is above 0.2.

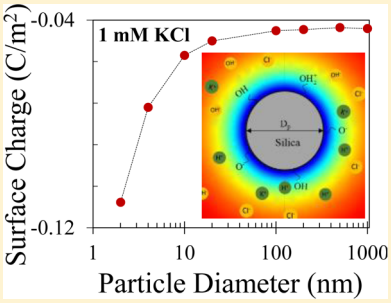

1. INTRODUCTION

Recent advances in micro-/nanotechnology attract significant attention to the use of nanoparticles in diverse ranges of applications including DNA analysis/sequencing systems,[1−9] DNA and protein transport,[10−14] drug delivery,[15−18] biological/chemical agent detection,[19,20] and micro-/nanochip sensors.[21−23] The performance of these devices relies on precise control and manipulation of various-sized nanoparticles in various ionic solutions. For example, manipulating the cellular uptake of nanoparticles has promised multiple biomedical applications, such as designing nanoparticles according to the dimensional limits for targeting and killing diseased cells.[24] Recent experiments demonstrated that reduced particle size does not necessarily increase the cellular uptake rate. Interestingly, certain-sized nanoparticles are internalized faster than the smaller ones by several cell types,[24−28] and such unexpected size dependent nanoparticle transport is not yet well understood.

When a particle is immersed in an aqueous medium, it becomes charged due to protonation/deprotonation on the particle surface.[29] The resulting surface charge interacting with dissolved ions forms the electrical double layer (EDL) surrounding the charged particle.[30] More counterions are accumulated, while co-ions are depleted within the EDL. Transport of nanoparticles highly depends on the particle's surface charge properties. For example, the process of nanoparticle translocation through a nanopore depends on the surface charge densities of the pore and the particle.[31−33] Due to the curvature effects, particle's surface charge also depends on its size.[34−39] However, most existing studies assume that the surface charge density of a particle is a material property independent of the particle size.[40−42] For example, Kreuter[40] studied nanoparticle-mediated delivery of drugs to the brain and characterized the transport of 20, 40, 60, and 80 nm diameter nanoparticles as a sole function of surfactant coating without considering the nanoparticle size effects. Similarly, nanoparticle−cell interactions were characterized based on the particle's surface-chemical properties while the size effects on 14, 30, 50, 74, and 100 nm nanoparticles' surface charges were not considered.[41] In addition, Lu et al.[42] studied nanoparticles in the range of 2−100 nm with different surface modifications and assumed constant particle charge in their characterization of particle−water interactions. Many previous studies assumed constant surface charge on particles, regardless of the particle size and solution properties (i.e., solution pH and salt concentration).[32,33,43,44] For example, electrokinetic transport of charged molecules in nanofluidic channels were studied by assuming a constant surface charge density, even though the background salt concentration and pH levels were varied during the experiments.[43] Similarly, DNA translocation that speeds through silica nanopores at different solution environments were directly related to surface charges; however, it is studied without considering the background salt concentration effects on charge densities.[44] The effects of electroosmotic flow on ionic rectification in asymmetric nanopores were also explored by varying the background salt concentration and without taking into account the effect of solution properties on the nanopore's surface charge.[32] Under certain conditions, such assumptions failed to explain the observed experimental results.[34,36,45] These assumptions are inaccurate and unrealistic since the nanoparticle surface charge density strongly depends

Received: October 24, 2013
Revised: January 7, 2014
Published: January 8, 2014

   dx.doi.org/10.1021/jp410536n | J. Phys. Chem. C 2014, 118, 1836−1842

on the particle size as well as the pH and the background ionic concentration.

The present study theoretically investigates the size dependent surface charge properties of silica nanoparticles immersed in an aqueous solution. The reason to choose silica nanoparticle as an example is because it has been widely used for ceramics, chromatography, catalysis, adsorption,[46−49] and carriers in biomolecular transport and drug delivery.[50,51] In contrast to the previous studies neglecting the surface chemistry, we considered the effects of the pH and salt concentration of the aqueous solution, the site density of the functional groups, and protonation/deprotonation surface reactions on the nanoparticle's surface charge. A multi-ion charge-regulation model[52] is employed for the first time to investigate the size dependent surface charges of silica nanoparticles as functions of salt concentrations and pH. The model is first validated by existing experimental data available from the literature.[34]

2. MATHEMATICAL MODEL

We considered a spherical nanoparticle of diameter D_p immersed in an infinite electrolyte medium, as shown in Figure 1. The background electrolyte contains N types of ionic

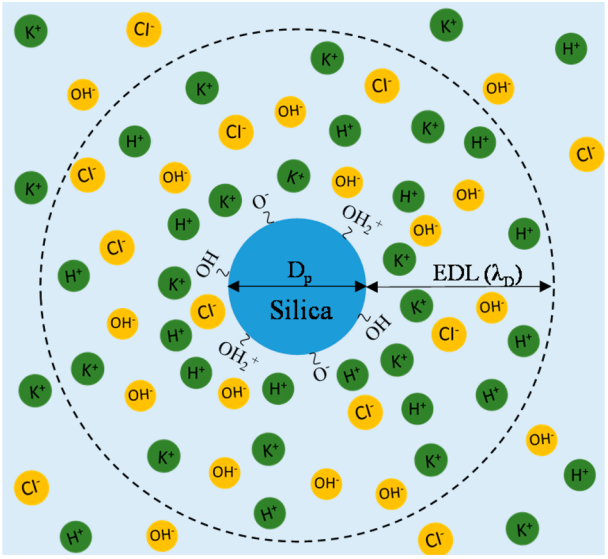

Figure 1. Schematic illustration of the functional groups on a silica nanoparticle.

species. We assume the electrolyte is made of KCl with bulk concentration C_{KCl}, and its pH is adjusted by KOH and HCl solutions. Consequently, there are four ionic species (i.e., N = 4), H^+, OH^-, K^+, and Cl^- dissolved in the solution. We assume that the silica nanoparticle's suface bears silanol functional groups. The particle becomes charged by the protonation/deprotonation processes. Figure 1 schematically shows a negatively charged silica nanoparticle,and ionic distributions in its EDL.

The ionic mass transport within the electrolyte is governed by the Poisson−Boltzmann (PB) equation,

$$\nabla^2\phi = -\frac{F}{\varepsilon_0\varepsilon_f}\sum_{i=1}^{4} z_i C_{i0}\exp\left(-\frac{z_i F\phi}{RT}\right) \tag{1}$$

where ϕ is the electric potential within the fluid; F is the Faraday constant; C_{i0} and z_i are the bulk molar concentration and valence of the ith ionic species (i = 1 for H^+, i = 2 for K^+, i = 3 for Cl^-, and i = 4 for OH^-), respectively; R is the university gas constant; T is the fluid temperature; ε_0 is the permittivity of vacuum; and ε_f is the relative permittivity of the electrolyte solution.

C_{i0} of each species satisfies the electroneutrality condition:

$$C_{10} = 10^{-pH+3} \quad \text{and} \quad C_{40} = 10^{-(14-pH)+3} \tag{2}$$

$$C_{20} = C_{KCl} \quad \text{and} \quad C_{30} = C_{KCl} + C_{10} - C_{40} \quad \text{when pH} \le 7 \tag{3}$$

$$C_{20} = C_{KCL} + C_{10} - C_{40} \quad \text{and} \quad C_{30} = C_{KCL} \quad \text{when pH} > 7 \tag{4}$$

Electric potential ϕ = 0, when $r\to\infty$. On the rigid nanoparticle surface, surface charge density boundary condition, $-\varepsilon_0\varepsilon_f\mathbf{n}\cdot\nabla\phi = \sigma$, is imposed.

Due to the protonation/deprotonation reactions of the dissociable functional groups at the solid/liquid interface, the nanoparticle surface reveals a charge-regulated nature. The surface charge density of the nanoparticle is modeled by the full multi-ion charge-regulation model.[52] To account for the charge regulation, we assume the following two protonation reactions of singly Si-coordinated sites with equilibrium constants K_A and K_B:

$$SiOH \leftrightarrow SiO^- + H^+ \tag{5}$$

$$SiOH + H^+ \leftrightarrow SiOH_2^+ \tag{6}$$

The equilibrium constants are calculated as

$$K_A = \frac{N_{SiO^-}[H^+]_s}{N_{SiOH}} \quad \text{and} \quad K_B = \frac{N_{SiOH_2^+}}{N_{SiOH}[H^+]_s} \tag{7}$$

where N_{SiOH}, N_{SiO^-}, and N_{SiOH2}^+, are the surface site densities of SiOH, SiO^-, and $SiOH_2^+$, respectively. $[H^+]_s$ is the concentration of H^+ ions at the solid/liquid interface and is governed by the Boltzmann distribution. Note that effects of the Stern layer in the vicinity of the charged silica nanoparticle are neglected in the current analysis. The total number site density of silanol functional groups on the solid/liquid interface is

$$N_{total} = N_{SiOH} + N_{SiO^-} + N_{SiOH_2^+} \tag{8}$$

Based on eqs 7 and 8, surface charge density of the nanoparticle can be expressed as

$$\sigma = -FN_{total}\frac{K_A - K_B[H^+]_s^2}{K_A + [H^+]_s + K_B[H^+]_s^2} \tag{9}$$

3. NUMERICAL IMPLEMENTATION AND CODE VALIDATION

The one-dimensional (1D) model in the spherical coordinate system is numerically solved using a commercial finite-element package, COMSOL Multiphysics (www.comsol.com), installed in a high-performance cluster. Since the field variables exponentially decay within the EDL of thickness λ_D,

$$\lambda_D = \sqrt{\varepsilon_0\varepsilon_f RT/\sum_{i=1}^{4} F^2 z_i^2 C_{i0}} \tag{10}$$

dx.doi.org/10.1021/jp410536n | J. Phys. Chem. C 2014, 118, 1836−1842

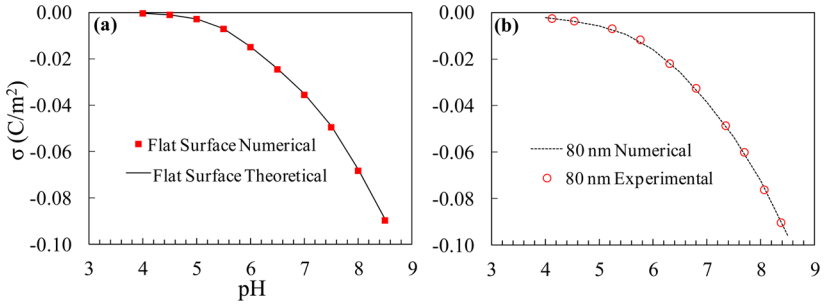

Figure 2. Surface charge densities of a planar silica surface (a) and 80 nm silica nanoparticle (b) as a function of pH. The theoretical result in panel a is from ref 52, while experimental data in panel b are from ref 34.

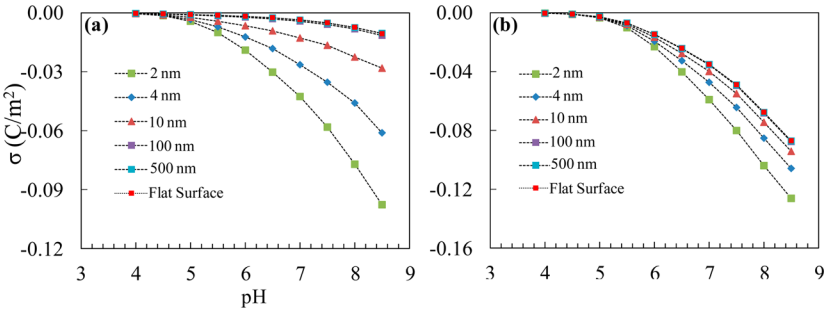

Figure 3. Surface charge density of silica nanoparticles of different sizes as a function of pH in 1 (a) and 100 mM (b) KCl solutions.

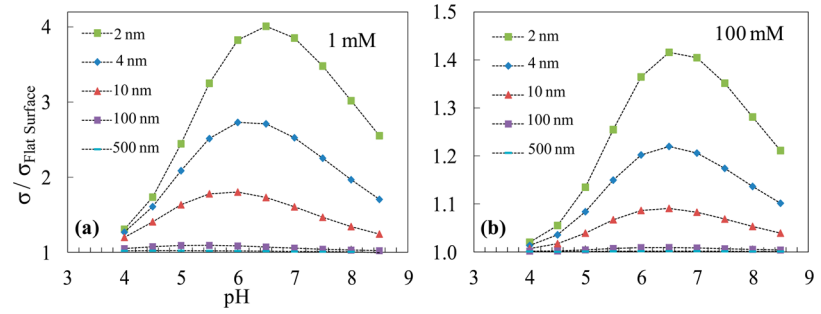

Figure 4. Normalized surface charge density as a function of pH in 1 (a) and 100 mM (b) KCl solutions.

all simulations used $d = D_p + 60\lambda_D$ as the far field boundary. Nonuniform mesh with finer mesh within the EDL is adopted. Physical parameters used in the simulations are $\varepsilon_0\varepsilon_f = 7.08 \times 10^{-10}$ F/m, $R = 8.31$ J/(mol·K), $F = 96490$ C/mol, $T = 300$ K, $N_{total} = 8$ sites/nm^2,[53] $pK_A = -\log K_A = 7.6$, and $pK_B = -\log K_B = 1.9$.

To validate our numerical procedure, we first modeled a flat silica surface in contact with a semi-infinite electrolyte solution. Analytical solution for the surface charge density of a planar surface has been recently derived by Yeh et al.[52] Figure 2a depicts the surface charge density of a planar surface as a function of pH for bulk $C_{KCl} = 100$ mM. Our numerical results (red squares) are in good agreement with the theoretical results (solid line). Clearly, the surface charge density increases with an increase in pH of the solution.

To further ensure that the model captures the underlying physics of the origin of interfacial charge, we also compare the model's prediction with the experimental data obtained from the literature.[34] Figure 2b depicts the surface charge density of a silica nanoparticle of 80 nm in diameter as a function of pH immersed in 100 mM KCl solution. The model's prediction (solid line) agrees well with the experimental data (red circles), confirming that the present model successfully captures the essential physics of the origin of the charge of silica nanoparticles. In the following we use the verified model to investigate the size dependent surface charge of silica nanoparticles as functions of pH and background salt concentration, C_{KCl}.

4. RESULTS AND DISCUSSION

4.1. Size Dependent Surface Charge Properties: pH Effect. Figure 3 depicts the surface charge densities of silica nanoparticles of different sizes as a function of pH for $C_{KCl} = 1$ mM (Figure 3a) and 100 mM (Figure 3b). For comparison, the surface charge density for a flat silica surface is also plotted. Under the same conditions, the surface charge density magnitude increases as pH increases. This behavior quantitatively agrees with the experimental observations as shown in Figure 2b, and also qualitatively agrees with the results from Yeh et al.,[52] Abbas et al.,[35] Behrens et al.,[36] Kobayashi et al.,[34] and Sonnefeld et al.[45] Variation of the surface charge with pH is expected. As the concentration of H^+ ions decreases with increased pH, more negatively charged SiO^- are dissociated from the functional groups SiOH resulting in higher negative surface charge density. Overall, Figure 3 clearly indicates that

dx.doi.org/10.1021/jp410536n | J. Phys. Chem. C 2014, 118, 1836−1842

the surface charge of silica nanoparticles also depends on their sizes. Under a fixed background salt concentration, the magnitude of the surface charge increases with decreased particle size, which is in qualitative agreement with the previous studies such as Yeh et al.,[52] Abbas et al.,[35] Behrens et al.,[36] and Gunnarsson et al.[37] However, the surface charge density becomes independent of the particle size after a critical diameter. This critical value also depends on the pH and salt concentration of the solution. For example, the critical particle diameter at pH = 6 is about 100 nm for C_{KCl} = 1 mM, while it is about 10 nm for C_{KCl} = 100 mM.

To clearly show the behavior of the size dependent surface charge density, the particle's surface charge density is normalized with that of a flat surface at a given pH value. Parts a and b of Figure 4 depict the normalized surface charge density as a function of pH for C_{KCl} = 1 and 100 mM, respectively. The normalized surface charge of particles larger than 100 nm is close to 1, suggesting that the particle size effects on the surface charge become insignificant when the particle size is larger than 100 nm under the considered conditions. For particles less than 100 nm, the normalized surface charge first increases with pH, attains a peak value at a critical pH value, and then decreases with further increases in pH. The critical pH value also depends on the particle's size. The critical pH value increases with decreased particle size. For example in 1 mM KCl solution, the critical pH for 2 nm particles is 6.5, while this is pH = 5.5 for 10 nm particles. In addition, the normalized surface charge density increases significantly with reduced particle size, implying that the surface charge density of the nanoparticles is significantly higher than that of a flat surface made of the same material.

The variation of the normalized surface charge density with pH can be explained by the concentration of H^+ ions on the particle surface. As pH level increases, the bulk concentration of H^+ ions decreases, resulting in lower concentration of H^+ ions and, accordingly, higher surface charge on the particle surface. Figure 5 depicts the surface concentration of H^+ ions on the particle surface normalized by that on a flat surface at the same conditions. The normalized surface concentration of H^+ ions is less than 1, implying that the concentration of H^+ ions on small particle's surface is lower than that on a flat surface. At the same pH level and background salt concentration, the surface concentration of H^+ ions decreases as the particle size decreases, leading to more negatively charged SiO^- dissociated from the functional groups SiOH and, therefore, higher negative surface charge density, as shown in Figure 3. For relatively small particles, the normalized surface concentration of H^+ ions decreases with increased pH and obtains a minimum at a certain pH value, above which it increases as the pH is further increased. Since the surface charge of the particle is inversely proportional to the surface concentration of $[H^+]$ ions, the normalized surface charge density increases with pH, attains a maximum, and then declines, as shown in Figure 4.

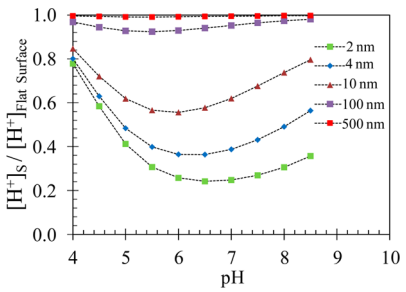

Figure 5. Normalized surface concentration of $[H^+]$ ions as a function of pH at C_{KCl} = 1 mM.

4.2. Size Dependent Surface Charge Properties: Background Salt Concentration Effect. Under the same pH and particle size, we found that the particle's surface charge density increases with an increase in the background salt concentration, which is in agreement with the experimental observations[34,36,54] and theoretical predictions.[35,55] Parts a and b of Figure 6 depict, respectively, the surface concentrations of H^+ and K^+ ions as a function of the background salt concentration for different particle sizes at pH = 6.5. Overall, an increase in salt concentration results in an increase in the concentration of K^+ ions and a decrease in the concentration of H^+ ions. For a fixed particle size, more K^+ ions are attracted to the negatively charged particle surface with increased background salt concentration. The increased number of K^+ ions exclude H^+ ions, resulting in lower concentration of H^+ ions on the particle surface, and accordingly higher negative surface charge density. At fixed salt concentration, the surface concentration of H^+ ions increases with the particle size and asymptotically reaches the value of the flat plate around particle diameter of 100 nm. At relatively low background salt concentrations, the surface concentration of H^+ ions significantly depends on the particle size.

To characterize the background salt concentration effects on the size dependent surface charge properties, Figure 7 depicts the normalized surface concentration of H^+ ions as a function of the particle diameter for C_{KCl} = 1, 10, and 100 mM at pH = 6.5. The normalization was done using the surface concentration of H^+ ions on a flat plate. For D_p > 100 nm, the normalized surface concentrations of H^+ ions are close to 1 for all salt concentrations. For particles smaller than 100 nm, the concentration of H^+ ions on smaller particles is lower, yielding higher negative surface charge. Such size dependence is more significant at lower salt concentrations.

Figure 8 shows the particle's surface charge density normalized by that of a flat surface as a function of the particle size at pH = 6.5. For all background salt concentrations, the normalized particle surface charge density decreases as the particle size increases. As explained before, this is attributed to the increase in the normalized surface concentration of the H^+ ions, as shown in Figure 7. For relatively small particles, the normalized surface charge density decreases with an increase in C_{KCl}. This is attributed to the increase in the surface concentration of H^+ ions with an increase in C_{KCl}, as shown in Figure 7.

Since both pH and salt concentration affect the bulk concentration of each ionic species, and accordingly the EDL thickness, the combined effects of pH and salt concentration on the size dependent surface charge density can be described by the ratio of EDL thickness (eq 10) to the particle diameter, λ_D/D_p. Figure 9 shows normalized surface charge density as a function of λ_D/D_p. The normalized surface charge density is close to 1 when λ_D/D_p < 0.2 and increases with increased λ_D/D_p. Therefore, regardless of the salt concentration and pH, the surface charge density is independent of the particle size when λ_D/D_p < 0.2. In the range of λ_D/D_p > 0.2, the surface charge density of the nanoparticle becomes size dependent and is higher than that of the flat surface made of the same material.

dx.doi.org/10.1021/jp410536n | J. Phys. Chem. C 2014, 118, 1836−1842

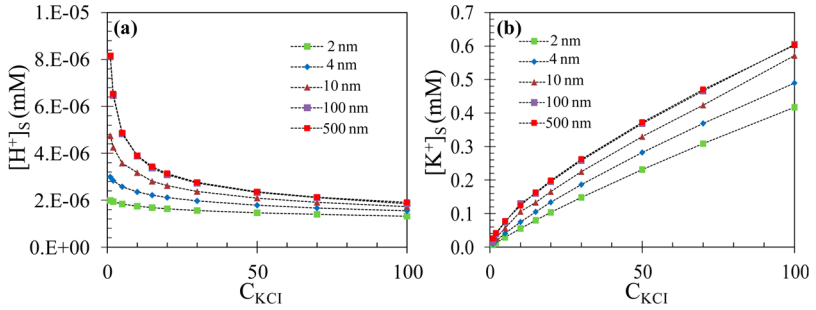

Figure 6. Surface concentrations of H^+ ions (a) and K^+ ions (b) as a function of C_{KCl} for different particle sizes at pH = 6.5 (where, for example, 1.E-05 represents 1×10^{-5}).

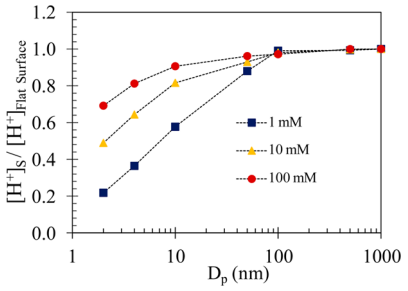

Figure 7. Normalized surface concentration of H^+ ions as a function of particle diameter for various background salt concentrations at pH = 6.5.

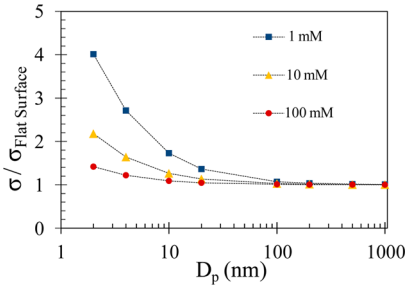

Figure 8. Normalized surface charge density as a function of particle diameter for various background salt concentrations at pH = 6.5.

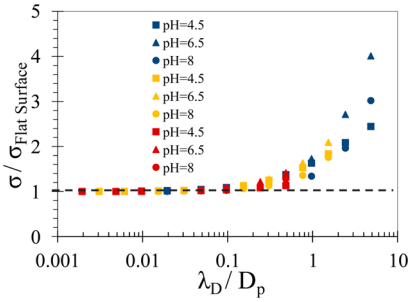

Figure 9. Normalized surface charge density as a function of the ratio of EDL thickness to the particle diameter. Different shapes represent different pH values, while different colors show different salt concentrations (blue, 1 mM; yellow, 10 mM; red, 100 mM).

5. CONCLUSION

Surface charge densities of spherical silica nanoparticles of different sizes are theoretically investigated as functions of pH and salt concentration. In contrast to most studies in the literature that assume constant surface charge density, the present model takes into account the charge regulation as functions of the solution properties. The Stern layer effects are still not considered in the current study and will be investigated in the future. The results demonstrate increased surface charge density for all particle sizes with increases of pH and salt concentration. Surface charge density decreases with increased particle size and asymptotically reaches that of a flat plate. This behavior depends on both pH and salt concentration. Variation of the surface charge with the particle size is attributed to the change in the surface concentration of H^+ ions. Particle diameter normalized with the EDL thickness is used to combine the effects of pH and salt concentration. In the range of $\lambda_D/D_p < 0.2$, one can neglect the effect of the particle size on its surface charge density, regardless of the pH and salt concentration. However, the surface charge density of silica nanoparticles becomes size dependent when $\lambda_D/D_p > 0.2$, and typically the magnitude of surface charge density increases with decreased particle size. These results can be used to explain why certain-sized nanoparticles are transported in nanopores faster than the smaller ones made out of the same material.[24−28]

AUTHOR INFORMATION

Corresponding Author

*Phone: (757) 683-3304. E-mail: sqian@odu.edu.

Author Contributions

§M.B. and S.A. contributed equally to this work.

Notes

The authors declare no competing financial interest.

REFERENCES

(1) Kasianowicz, J. J.; Brandin, E.; Branton, D.; Deamer, D. W. Characterization of individual polynucleotide molecules using a membrane channel. *Proc. Natl. Acad. Sci. U. S. A.* **1996**, *93*, 13370−13773.

(2) Min, S. K.; Kim, W. Y.; Cho, Y.; Kim, K. S. Fast DNA sequencing with a graphene-based nanochannel device. *Nat. Nanotechnol.* **2011**, *6*, 162−165.

(3) Meller, A.; Nivon, L.; Branton, D. Voltage-Driven DNA Translocations through a Nanopore. *Phys. Rev. Lett.* **2001**, *86*, 3435−3438.

(4) Keyser, U. F.; Koeleman, B. N.; Van Dorp, S.; Krapf, D.; Smeets, R. M.; Lemay, S. G.; Dekker, N. H.; Dekker, C. Direct force measurements on DNA in a solid-state nanopore. *Nat. Phys.* **2006**, *2*, 473−477.

(5) Kowalczyk, S. W.; Wells, D. B.; Aksimentiev, A.; Dekker, C. Slowing down DNA Translocation through a Nanopore in Lithium Chloride. *Nano Lett.* **2012**, *12*, 1038−1044.

(6) Stein, D.; Deurvorst, Z.; van der Heyden, F. H.; Koopmans, W. J.; Gabel, A.; Dekker, C. Electrokinetic Concentration of DNA Polymers in Nanofluidic Channels. *Nano Lett.* **2010**, *10*, 765−772.

(7) Li, J.; Gershow, M.; Stein, D.; Brandin, E.; Golovchenko, J. DNA molecules and configurations in a solid-state nanopore microscope. *Nat. Mater.* **2003**, *2*, 611−615.
(8) Chen, P.; Gu, J.; Brandin, E.; Kim, Y. R.; Wang, Q.; Branton, D. Probing Single DNA Molecule Transport Using Fabricated Nanopores. *Nano Lett.* **2004**, *4*, 2293−2298.
(9) Taton, T. A.; Mirkin, C. A.; Letsinger, R. L. Scanometric DNA Array Detection with Nanoparticle Probes. *Science* **2000**, *289*, 1757−1760.
(10) Ravi Kumar, M. N. V.; Bakowsky, U.; Lehr, C. Preparation and characterization of cationic PLGA nanospheres as DNA carriers. *Biomaterials* **2004**, *25*, 1771−1777.
(11) Mao, H. Q.; Roy, K.; Troung-Le, V. L.; Janes, K. A.; Lin, K. Y.; Wang, Y.; August, J. T.; Leong, K. W. Chitosan-DNA nanoparticles as gene carriers: synthesis, characterization and transfection efficiency. *J. Controlled Release* **2001**, *70*, 399−421.
(12) Calvo, P.; Remunan-Lopez, C.; Vila-Jato, J.; Alonso, M. Chitosan and Chitosan/Ethylene Oxide-Propylene Oxide Block Copolymer Nanoparticles as Novel Carriers for Proteins and Vaccines. *J. Appl. Polym. Sci.* **1997**, *63*, 125−132.
(13) Kneuer, C.; Sameti, M.; Haltner, E. G.; Schiestel, T.; Schirra, H.; Schmidt, H.; Lehr, C. M. Silica nanoparticles modified with aminosilanes as carriers for plasmid DNA. *Int. J. Pharm. (Amsterdam, Neth.)* **2000**, *196*, 257−261.
(14) Roy, K.; Mao, H. Q.; Huang, S. K.; Leong, K. W. Oral gene delivery with chitosan−DNA nanoparticles generates immunologic protection in a murine model of peanut allergy. *Nat. Med. (N. Y., NY, U. S.)* **1999**, *5*, 387−391.
(15) Kowalczyk, S. W.; Hall, A. R.; Dekker, C. Detection of Local Protein Structures along DNA Using Solid-State Nanopores. *Nano Lett.* **2009**, *10*, 324−328.
(16) Yusko, E. C.; Johnson, J. M.; Majd, S.; Prangkio, P.; Rollings, R. C.; Li, J.; Yang, J.; Mayer, M. Controlling protein translocation through nanopores with bio-inspired fluid walls. *Nat. Nanotechnol.* **2011**, *6*, 253−260.
(17) Han, A.; Creus, M.; Schürmann, G.; Linder, V.; Ward, T. R.; de Rooij, N. F.; Staufer, U. Label-Free Detection of Single Protein Molecules and Protein−Protein Interactions Using Synthetic Nanopores. *Anal. Chem.* **2008**, *80*, 4651−4658.
(18) Kaasalainen, M.; Mäkilä, E.; Riikonen, J.; Kovalainen, M.; Järvinen, K.; Herzig, K. H.; Lehto, V. P.; Salonen, J. Effect of isotonic solutions and peptide adsorption on zeta potential of porous silicon nanoparticle drug delivery formulations. *Int. J. Pharm. (Amsterdam, Neth.)* **2012**, *431*, 230−236.
(19) Lan, W. J.; Holden, D. A.; Liu, J.; White, H. S. Pressure-Driven Nanoparticle Transport across Glass Membranes Containing a Conical-Shaped Nanopor. *J. Phys. Chem. C* **2011**, *115*, 18445−18452.
(20) Lan, W. J.; Holden, D. A.; Zhang, B.; White, H. S. Nanoparticle Transport in Conical-Shaped Nanopores. *Anal. Chem.* **2011**, *83*, 3840−3847.
(21) Dekker, C. Solid-state nanopores. *Nat. Nanotechnol.* **2007**, *2*, 209−215.
(22) Howorka, S.; Cheley, S.; Bayley, H. Sequence-specific detection of individual DNA strands using engineered nanopores. *Nat. Biotechnol.* **2001**, *19*, 636−639.
(23) Howorka, S.; Siwy, Z. Nanopore analytics: sensing of single molecules. *Chem. Soc. Rev.* **2009**, *38*, 2360−2384.
(24) Redhead, H.; Davis, S.; Illum, L. Drug delivery in poly (lactide-co-glycolide) nanoparticles surface modified with poloxamer 407 and poloxamine 908: In vitro characterisation and in vivo evaluation. *J. Controlled Release* **2001**, *70*, 353−363.
(25) Varela, J. A.; Bexiga, M. G.; Åberg, C.; Simpson, J. C.; Dawson, K. A. Quantifying size-dependent interactions between fluorescently labeled polystyrene nanoparticles and mammalian cells. *J. Nanobiotechnol.* **2012**, *10*, 1−6.
(26) Chithrani, B. D.; Ghazani, A. A.; Chan, W. C. Determining the size and shape dependence of gold nanoparticle uptake into mammalian cells. *Nano Lett.* **2006**, *6*, 662−668.
(27) Chithrani, B. D.; Chan, W. C. Elucidating the mechanism of cellular uptake and removal of protein-coated gold nanoparticles of different sizes and shapes. *Nano Lett.* **2007**, *7*, 1542−1550.
(28) Sabuncu, A. C.; Grubbs, J.; Qian, S.; Abdel-Fattah, T. M.; Stacey, M. W.; Beskok, A. Probing nanoparticle interactions in cell culture media. *Colloids Surf., B* **2012**, *95*, 96−102.
(29) Hunter, R. J. *Zeta potential in colloid science: principles and applications*; Academic Press: London, 1981.
(30) Masliyah, J. H.; Bhattacharjee, S. *Electrokinetic and colloid transport phenomena*; John Wiley & Sons: Hoboken, NJ, 2006.
(31) Actis, P.; Vilozny, B.; Seger, R. A.; Li, X.; Jejelowo, O.; Rinaudo, M.; Pourmand, N. Voltage-controlled metal binding on polyelectrolyte-functionalized nanopores. *Langmuir* **2011**, *27*, 6528−6533.
(32) Ai, Y.; Zhang, M.; Joo, S. W.; Cheney, M. A.; Qian, S. Effects of electroosmotic flow on ionic current rectification in conical nanopores. *J. Phys. Chem. C* **2010**, *114*, 3883−3890.
(33) Ali, M.; Yameen, B.; Cervera, J.; Ramírez, P.; Neumann, R.; Ensinger, W.; Knoll, W.; Azzaroni, O. Layer-by-layer assembly of polyelectrolytes into ionic current rectifying solid-state nanopores: insights from theory and experiment. *J. Am. Chem. Soc.* **2010**, *132*, 8338−8348.
(34) Kobayashi, M.; Juillerat, F.; Galletto, P.; Bowen, P.; Borkovec, M. Aggregation and charging of colloidal silica particles: Effect of particle size. *Langmuir* **2005**, *21*, 5761−5769.
(35) Abbas, Z.; Labbez, C.; Nordholm, S.; Ahlberg, E. Size-dependent surface charging of nanoparticles. *J. Phys. Chem. C* **2008**, *112*, 5715−5723.
(36) Behrens, S. H.; Christl, D. I.; Emmerzael, R.; Schurtenberger, P.; Borkovec, M. Charging and aggregation properties of carboxyl latex particles: Experiments versus DLVO theory. *Langmuir* **2000**, *16*, 2566−2575.
(37) Gunnarsson, M.; Abbas, Z.; Ahlberg, E.; Nordholm, S. Corrected Debye−Hückel analysis of surface complexation: III. Spherical particle charging including ion condensation. *J. Colloid Interface Sci.* **2004**, *274*, 563−578.
(38) Wang, Z. W.; Li, G. Z.; Guan, D. R.; Yi, X. Z.; Lou, A. J. The surface potential of a spherical colloid particle: Functional theoretical approach. *J. Colloid Interface Sci.* **2002**, *246*, 302−308.
(39) Ohshima, H. Surface Charge Density/Surface Potential Relationship for a Spherical Colloidal Particle in a Salt-Free Medium. *J. Colloid Interface Sci.* **2002**, *247*, 18−23.
(40) Kreuter, J. Influence of the surface properties on nanoparticle-mediated transport of drugs to the brain. *J. Nanosci. Nanotechnol.* **2004**, *4*, 484−488.
(41) Verma, A.; Stellacci, F. Effect of surface properties on nanoparticle−cell interactions. *Small* **2010**, *6*, 12−21.
(42) Lu, Y.; Yin, Y.; Mayers, B. T.; Xia, Y. Modifying the surface properties of superparamagnetic iron oxide nanoparticles through a sol-gel approach. *Nano Lett.* **2002**, *2*, 183−186.
(43) Oh, Y. J.; Garcia, A. L.; Petsev, D. N.; Lopez, G. P.; Brueck, S. R.; Ivory, C. F.; Han, S. M. Effect of wall−molecule interactions on electrokinetic transport of charged molecules in nanofluidic channels during FET flow control. *Lab Chip* **2009**, *9*, 1601−1608.
(44) He, Y.; Tsutsui, M.; Fan, C.; Taniguchi, M.; Kawai, T. Controlling DNA translocation through gate modulation of nanopore wall surface charges. *ACS Nano* **2011**, *5*, 5509−5518.
(45) Sonnefeld, J.; Löbbus, M.; Vogelsberger, W. Determination of electric double layer parameters for spherical silica particles under application of the triple layer model using surface charge density data and results of electrokinetic sonic amplitude measurements. *Colloids Surf., A* **2001**, *195*, 215−225.
(46) Popat, A.; Hartono, S. B.; Stahr, F.; Liu, J.; Qiao, S. Z.; Lu, G. Q. M. Mesoporous silica nanoparticles for bioadsorption, enzyme immobilisation, and delivery carriers. *Nanoscale* **2011**, *3* (7), 2801−2818.
(47) Yang, X.; Shen, Z.; Zhang, B.; Yang, J.; Hong, W. X.; Zhuang, Z.; Liu, J. Silica nanoparticles capture atmospheric lead: Implications in the treatment of environmental heavy metal pollution. *Chemosphere* **2013**, *90*, 653−659.

(48) Y Darvishi Cheshmeh Soltani, R.; Khataee, A. R.; Safari, M.; Joo, S. W. Preparation of bio-silica/chitosan nanocomposite for adsorption of a textile dye in aqueous solutions. *Int. Biodeterior. Biodegrad.* **2013**, *85*, 383−391.
(49) Li, X.; Zhang, J.; Gu, H. Adsorption and desorption behaviors of DNA with magnetic mesoporous silica nanoparticles. *Langmuir* **2011**, *27*, 6099−6106.
(50) Bharti, B.; Meissner, J.; Findenegg, G. H. Aggregation of silica nanoparticles directed by adsorption of lysozyme. *Langmuir* **2011**, *27*, 9823−9833.
(51) Thomassen, L. C.; Rabolli, V.; Masschaele, K.; Alberto, G.; Tomatis, M.; Ghiazza, M.; Turci, F.; Breynaert, E.; Martra, G.; Kirschhock, C. E. Model system to study the influence of aggregation on the hemolytic potential of silica nanoparticles. *Chem. Res. Toxicol.* **2011**, *24*, 1869−1875.
(52) Yeh, L.-H.; Xue, S.; Joo, S. W.; Qian, S.; Hsu, J. P. Field effect control of surface charge property and electroosmotic flow in nanofluidics. *J. Phys. Chem. C* **2012**, *116*, 4209−4216.
(53) Andersen, M. B.; Frey, J.; Pennathur, S.; Bruus, H. Surface-dependent chemical equilibrium constants and capacitances for bare and 3-cyanopropyldimethylchlorosilane coated silica nanochannels. *J. Colloid Interface Sci.* **2011**, *353*, 301−310.
(54) Dunér, G.; Iruthayaraj, J.; Daasbjerg, K.; Pedersen, S. U.; Thormann, E.; Dėdinaitė, A. Attractive double-layer forces and charge regulation upon interaction between electrografted amine layers and silica. *J. Colloid Interface Sci.* **2012**, *385*, 225−234.
(55) Yeh, L. H.; Zhang, M.; Hu, N.; Joo, S. W.; Qian, S.; Hsu, J. P. Electrokinetic ion and fluid transport in nanopores functionalized by polyelectrolyte brushes. *Nanoscale* **2012**, *4*, 5169−5177.